View metadata, citation and similar papers at core.ac.uk

brought to you by CORE

provided by ScholarWorks@UNIST

Nuclear Engineering and Technology 52 (2020) 1963–1973

Contents lists available at ScienceDirect

Nuclear Engineering and Technology

journal homepage: www.elsevier.com/locate/net

Original Article

Experimental validation of simulating natural circulation of liquid metal using water

Min Ho Lee [a], Dong Wook Jerng [b, **], In Cheol Bang [a, *]

[a] Department of Nuclear Engineering, Ulsan National Institute of Science and Technology (UNIST), 50 UNIST-gil, Ulju-gun, Ulsan, 44919, Republic of Korea
[b] School of Energy Systems Engineering, Chung Ang Univ. Rep. of Korea, 84 Heukseok-ro, Dongjak-gu, Seoul, 06974, Republic of Korea

ARTICLE INFO

Article history:
Received 3 December 2019
Received in revised form
28 February 2020
Accepted 7 March 2020
Available online 16 March 2020

Keywords:
Liquid metal
Natural circulation
Similarity law
Modified Boussinesq number

ABSTRACT

Liquid metal-cooled reactors use various passive safety systems driven by natural circulation. Investigating these safety systems experimentally is more advantageous by using a simulant. Although numerous experimental approaches have been applied to natural circulation-driven passive safety systems using simulants, there has been no clear validation of the similarity law. To validate the similarity law experimentally, SINCRO-V experiment was conducted using Wood's metal and water for simulant of the Wood's metal. A pair of SINCRO-V facilities with length-scale ratio of 14.1:1 for identical Bo' was investigated, which was the main similarity parameter in temperature field simulation. In the experimental range of 0.2–1.0% of decay heat, the temperature distribution characteristics of the small water facility were very similar to that of the large Wood's metal facility. The temperature of the Wood's metal predicted by the water experiment showed good agreement with the actual Wood's metal temperature. Despite some error factors like discordance of *Gr*' and property change along the temperature, the water experiment predicted the Wood's metal temperature with an error of 27%. The validity of the similarity law was confirmed by the SINCRO-V experiments.

© 2020 Korean Nuclear Society, Published by Elsevier Korea LLC. This is an open access article under the CC BY-NC-ND license (http://creativecommons.org/licenses/by-nc-nd/4.0/).

1. Introduction

Passiveness of the safety system is one of the most important lessons from the Fukushima accident. As a result, various passive safety systems have been researched and applied to nuclear reactors. Changes in the nuclear safety regime have also been applied to reactors under development, such as sodium-cooled fast reactor (SFR) and lead-cooled fast reactor (LFR). The SFR and LFR employ a liquid metal as their coolant, which has superior thermal characteristics compared with the conventional coolant, i.e., water. Therefore, liquid metal-cooled reactors (LMRs) have the advantage of utilizing natural circulation, which could provide full passiveness to the safety system.

Various passive safety systems for LMRs have been developed based on natural circulation. The Experimental Breeder Reactor-II (EBR-II) is an SFR with a natural circulation shutdown cooler that can remove 0.6% of the total power [1]. In the event of accidents such as the loss of heat sink or flow, the shutdown cooler has sufficient cooling capability for reactor safety [1–3]. Monju is a prototype SFR. A passive safety system called auxiliary cooling system (ACS), or intermediate reactor ACS is connected to the intermediate heat exchanger, which removes decay heat by natural circulation [4,5]. Joyo, another prototype SFR (PGSFR), has also an auxiliary air-cooling system in addition to the original dump heat exchanger, and decay heat is removed by natural circulation of sodium [6]. The prototype Generation-IV SFR has a passive decay heat removal system (PDHRS) and reactor vessel ACS (RVACS) that provide passive cooling in addition to active safety systems [7]. The combination of active and passive safety systems can remove heat sufficiently, even during an accident without reactor shutdown [8]. The Advanced Sodium Technological Reactor for Industrial Demonstration (ASTRID) is under development, which is designed to have multiple decay heat removal systems, including systems using natural circulation [9]. Both the small, sealed, transportable, autonomous reactor (SSTAR) and European Lead-Cooled Training Reactor (ELECTRA) are LFRs that use natural circulation as the heat transfer mode even in normal operations along with decay heat removal to eliminate the need for pumps [10,11]. The Multipurpose Hybrid Research Reactor for High-tech Applications (MYRRAH) also

* Corresponding author.
** Corresponding author.
E-mail addresses: dwjerng@cau.ac.kr (D.W. Jerng), icbang@unist.ac.kr (I.C. Bang).

https://doi.org/10.1016/j.net.2020.03.005
1738-5733/© 2020 Korean Nuclear Society, Published by Elsevier Korea LLC. This is an open access article under the CC BY-NC-ND license (http://creativecommons.org/licenses/by-nc-nd/4.0/).

adopted an emergency cooling system that does not require pumps for operation [12].

In summary, various LMRs have adopted safety systems operated by natural circulation, and their performance should be analyzed. However, liquid metals have many problems such as toxicity, high temperature, large systems, etc. Lead and lead alloy are toxic and heavy. Because of this toxicity, additional protections such as isolation and filtering systems are necessary. Heavy weight requires the system to possess sufficient strength and thickness for containing them. Sodium is extremely reactive to other materials, including water and air. In addition to these practical difficulties, to secure similarity, the scale of the liquid metal system cannot be significantly reduced compared with the original system [13,14]. The large system corresponds to a high level of power and is also expensive. Thus, few studies have experimented with liquid metal. Ono et al. examined sodium in a plant dynamic testing loop facility to analyze the performance of the DHRS [15] in the actual geometry. For lead-bismuth, there have been only fundamental experiments in the 1-D loop [16–18].

Owing to the aforementioned difficulties in liquid metal experiments, most experimental research has been conducted using simulants. The basis of similarity was proposed by Grewal et al.; they suggested that water simulation of sodium natural circulation is better than the scaled sodium test [19]. Preliminary analysis of the design concept was conducted by comparing scaled and working fluids in terms of nondimensional numbers [14]. It was revealed that a similar experiment using water has many advantages over liquid metal experiments in reduced scale. Eguchi et al. evaluated the similarity law by comparing water experiments and computational fluid dynamics (CFD) data. The temperature showed 7%–30% discrepancy with CFD data because of insulation [20].

Water simulation experiments on the natural circulation of sodium have been conducted based on the similarity law. RAMONA and NEPTUN are two experimental facilities used to investigate natural circulation in direct heat exchanger (DHX) operation conditions, which were scaled-down by 1/20 and 1/5, respectively [21–24]. Various simulations of upper internal structures were conducted in RAMONA. The NEPTUN experiment showed similar results as that of RAMONA except for the reverse flow in the outer core region, which was called inter-wrapper flow. Water experiment with the 1/8 scaled-down model showed good agreement with temperature drop rate; however, the temperature gradient did not match actual plant data [13]. Akutsu et al. experimented with the same 1/8 model. The direct reactor ACS and primary reactor ACS were tested, and the data were used to develop multidimensional analysis codes [25]. Takeda et al. performed water experiment on a 1/20, 2-D slab model and observed the fluctuations of both velocity and temperature [26]. After the 2-D model experiment, they extended their work to the 3-D model, which had 1/20 and 1/6 scale, and compared the results [27]. They concluded that the effect of the modified Grashof number (*Gr*') was negligible, while that of modified Boussinesq number (Bo') was not. In AQUARIUS, which has 2-D slab shape in 1/20 scale, the effect of DHX location was investigated [28]. Recently, the spatial distribution of the phenomena was investigated by Mente et al. [29]. Flow distribution under DHX operation was observed and fuel assemblies in the outer core were more effectively cooled by direct downward flow from the DHX. The similarity law was also applied to loop-type reactors. The primary flow rate and temperature were investigated in a 1/10 scaled-down facility of a reactor named Japanese SFR [30]. The PHEASANT facility focused on velocity distribution as well as temperature, and visualized flow during DHX operation conditions [31]. In the case of LFR, the MYRRAHABELLE facility has been developed, which is a 1/5-scale 3D model of the MYRRHA, and temperature behavior in various transient situations were investigated [32].

To date, numerous experiments have been conducted based on the similarity law. However, the similarity law has not been sufficiently proven. At first sight, it appears illogical to simulate liquid metal, which has an extremely low Prandtl number (Pr), using water which has high Pr. To address this issue, there has been some research on the validation of the similarity law. Tanaka et al. and Hoffman et al. compared water data and actual plant temperature [13,22], focusing on qualitative phenomena and indirect parameters such as temperature gradient or drop rate. Eguchi et al. compared water data and numerical sodium data [20]. Although data was quantitatively compared, sodium data had inherent limitations and uncertainty because these were obtained by numerical method. Moreover, these discussions on the similarity law were conducted under DHX operation conditions. Therefore, the similarity law should be validated experimentally. In the present study, the similarity law between liquid metal and other fluids with relatively high Pr was validated in terms of temperature distribution. The temperature obtained by the liquid metal experiment and liquid metal temperature obtained by water experiment were directly compared at the same points.

2. Experimental methods

The thermal hydraulic characteristics of natural circulation can be characterized by several nondimensional numbers. In this section, various nondimensional numbers from the nondimensionalization of the governing equation are discussed, and the overall experimental design will be introduced.

2.1. Revisiting scaling law

The governing equations for natural convection are written below. These are mass, momentum, and energy conservation equations. Difference between equation (3) and (3-1) was existence of the heat source term as $Q_0/\rho c_p$ and sink term as $Q''/\rho c_p L$, which describes temperature change at the unit volume of the heating or cooling region respectively. For the heating region or cooling region, (3) was applied, and for the other regions, (3–1) was applied.

$$\frac{\partial u_i}{\partial x_i} = 0 \tag{1}$$

$$\frac{\partial u_i}{\partial t} + u_j \frac{\partial u_i}{\partial x_j} = \nu \frac{\partial^2 u_i}{\partial x_j^2} - \beta \Delta T g \delta_{i3} - \frac{1}{\rho} \frac{\partial P}{\partial x_i} \tag{2}$$

$$\frac{\partial T}{\partial t} + u_j \frac{\partial T}{\partial x_j} = \alpha \frac{\partial^2 T}{\partial x_j^2} + \frac{Q_0}{\rho c_p} - \frac{Q''}{\rho c_p L} \tag{3}$$

$$\frac{\partial T}{\partial t} + u_j \frac{\partial T}{\partial x_j} = \alpha \frac{\partial^2 T}{\partial x_j^2} \tag{3 -1}$$

To conduct nondimensionalization of the governing equations, the reference for each parameter was needed. However, unlike forced convection, there is no reference for some parameters in natural convection. Unlike the length scale which was clearly given, parameters like temperature, time, and velocity have no clear reference. To provide references for these parameters, the force balance between kinetic energy and buoyancy potential energy, and balance between heating and cooling by convection were employed. From the balance between buoyancy potential energy and kinetic energy, Richardson number was automatically determined as unity. And balance between heating rate and convective cooling made non-dimensional heating term as unity. As a result,

velocity, temperature difference, and time can be expressed as a function of the properties of the working fluid, geometry, and heating intensity in equations (4)–(6), respectively.

$$u_{ref} = \left(\frac{\beta g}{\rho c_p L}\right)^{1/3} Q^{1/3} \tag{4}$$

$$t_{ref} = \left(\frac{\rho c_p L^4}{\beta g}\right)^{1/3} Q^{-1/3} \tag{5}$$

$$\Delta T_{ref} = \left(\beta g \rho^2 c_p^2 L^5\right)^{-1/3} Q^{2/3} \tag{6}$$

Using these references, the governing equations can be non-dimensionalized, resulting in equations (7)–(9), and (9-1). Here, the heat source term could be treated as 1 (unity) if volumetric heat generation rate was maintained. The volumetric heat generation was set as the same for convenience. So that the heat source term in equation (9) was automatically evaluated as unity by assumption that Richardson number was unity, convective cooling is balanced with heating rate and the identical volumetric heat generation rate. The heat sink term could be considered in two ways. First, in the aspect of the overall system, heat flux could be expressed in the form of the total power over area if heat balance of the system maintained, like (Q_0L^3/L^2). And this term could be reduced to Q_0L and the heat sink term has the same form with the heat source term. Here, isotropic scaling was assumed in the expression of Q″ in another form and reduction. Thus, in the aspect of the overall system, similarity of the cooling boundary condition could be automatically achieved by isotropic scale reduction. Second, for heat transfer phenomena near boundary, heat flux term could be expressed as $k\Delta T_{ref}/L$, using the concept of the Fourier's law. Thereby, the heat sink term could be reduced to ($\alpha/u_{ref}L$). By using relationship between u_{ref} and t_{ref}, it could be changed to ($\alpha t_{ref}/L^2$), which is the same form with Fourier number. Fourier number means the ratio between the amount of the heat transfer to heat storage, thus, it should have value as 1 for both Wood's metal and water under steady state. Even under unsteady state, it could have the same value for both Wood's metal and water. By replacing u_{ref} to its definition in equation (4), the heat sink term summarized as $Bo'^{3/2}$, which could be identical between Wood's metal and water by matching the main similarity criterion for the similarity law, Bo'. Here, ΔT and Δx term in the Fourier's law was expressed by the ΔT_{ref} and L, which is reference temperature difference and length scale. It means that temperature profile in the cooling boundary should be linearly proportional to the reference temperature difference, and boundary layer thickness should be reduced in the isotropic manner, having same reduction ratio with the general length. In summary, similarity of the cooling region could be achieved by isotropic scale reduction, matching Bo' and assumption of temperature profile and thickness of the boundary layer. Even it could be valid under unsteady state if heat balance of the system is maintained.

$$\frac{\partial u_i^*}{\partial x_i^*} = 0 \tag{7}$$

$$\frac{\partial u_i^*}{\partial t^*} + u_j^* \frac{\partial u_i^*}{\partial x_j^*} = \frac{1}{Gr'^{1/2}} \frac{\partial^2 u_i^*}{\partial x_j^{2*}} - \frac{\beta g \Delta T_{ref} L}{u_{ref}^2} T^* \delta_{i3} - \frac{\Delta P}{\rho u_0^2} \frac{\partial P^*}{\partial x_i^*} \tag{8}$$

$$\frac{\partial T^*}{\partial t^*} + u_j^* \frac{\partial T^*}{\partial x_j^*} = \frac{1}{Bo'^{1/2}} \frac{\partial^2 T^*}{\partial x_j^{2*}} + \frac{Q_0 L}{\rho c_p u_{ref} \Delta T_{ref}} - \frac{Q''}{\rho c_p u_{ref} \Delta T_{ref}} \tag{9}$$

$$\frac{\partial T^*}{\partial t^*} + u_j^* \frac{\partial T^*}{\partial x_j^*} = \frac{1}{Bo'^{1/2}} \frac{\partial^2 T^*}{\partial x_j^{2*}} \tag{9 -1}$$

Two important numbers were derived from the diffusion terms on the right-hand side of equations (8) and (9): the modified *Gr*' and modified Bo'. Their definitions are given in equations (10) and (11), respectively. Between *Gr*' and Bo', with regard to the temperature field of natural circulation, Bo' is more important because it denotes the ratio of the amount of heat transferred by natural circulation to that of conduction. It is known that identical Bo' with compromised *Gr*' condition ensures the similarity of the temperature field [13,20,22].

$$Gr' = \left(\frac{\beta g}{\rho c_p}\right)^{2/3} \frac{L^{4/3} Q^{2/3}}{\nu^2} \tag{10}$$

$$Bo' = \left(\frac{\beta g}{\rho c_p}\right)^{2/3} \frac{L^{4/3} Q^{2/3}}{\alpha^2} \tag{11}$$

In general, the Rayleigh number has been used for natural circulation heat transfer. It indicates the intensity of natural circulation and determines heat transfer characteristics. However, the objective of this approach is the reproduction of the temperature field and not heat transfer performance. Therefore, rather than traditional natural convection, which focuses on the heat transfer coefficient at the boundary, reproducing the temperature distribution is the main objective of the Bo'-based similarity law. Thus, Bo' is more appropriate than the Rayleigh number, and the experiment was designed based on Bo'.

Temperature data in the simulating experiment can be interpreted to that of liquid metal. In this experiment, Wood's metal temperature was predicted by water experiment using reference temperature in equation (6). As previously mentioned, the reference parameter is the representative magnitude of a certain parameter. In other words, the temperature can be expressed by multiplying the reference parameter and non-dimensionalized temperature difference as in equations (13) and (14). The definition of the non-dimensionalized temperature difference θ was described in equation (12). It had basically the same meaning to the T* in equation (9), however, θ had a specific temperature point for calculation of the temperature difference, as boundary temperature.

$$\theta = \frac{T - T_{boundary}}{\Delta T_{ref}} \tag{12}$$

$$\Delta T_{Wood's\ metal} = \Delta T_{reference,\ Wood's\ metal} \times \theta_{Wood's\ metal} \tag{13}$$

$$\Delta T_{water} = \Delta T_{reference,\ water} \times \theta_{water} \tag{14}$$

$\theta_{Wood's\ metal}$ and θ_{water} can be matched by identical Bo'. In this regard, the Wood's metal temperature can be predicted by water temperature using the ratio of the reference temperature. Finally, temperature interpretation can be summarized as equation (15).

$$\Delta T_{Wood's\ metal} = \frac{\Delta T_{reference,\ Wood's\ metal}}{\Delta T_{reference,\ water}} \times \Delta T_{water} \tag{15}$$

2.2. Selection of working fluid

As discussed in the previous section, Bo' is the most important non-dimensional number for simulating the temperature field in natural circulation. In fact, in the definition of the Bo', there were two variables: the length scale and the total power. However, volumetric heat generation rate and corresponding total power was fixed in the SINCRO-V experiment. Because increase of the volumetric heat generation rate was limited by the specification of the cartridge heater and decrease of the volumetric heat generation rate provided only small advantage in scaling ratio and huge increase in the error of the predicted temperature. Therefore, Bo' is the solely function of the length scale. Candidates for the representative fluid for the liquid metal and nonmetallic fluid are shown in Fig. 1. The scale is defined as the relative length scale to obtain the same Bo' with water; therefore, water was set to 1 as reference. If the relative length scale is less than 1, then the size of the system should be smaller than that of the water and vice versa. Compared with water, metals have much higher thermal diffusivity, which is in the denominator of equation (11). The effects of other properties are less significant than that of thermal diffusivity. Therefore, the size of the metal system should be larger than the water system because size is in the numerator in equation (11).

To reduce distortion by scale, the difference of the length scale between two fluids should be minimized. Among liquid metals, mercury has the smallest difference of the length scale with nonmetallic fluid. However, mercury is toxic to the human body and the environment. Field's metal was also excluded owing to an economic issue. Between Cerrolow136 and Wood's metal, which have similar values of the length scale, Wood's metal was selected because of previous operation experience. There are four kinds of simulation fluid: heat transfer oil, heat transfer salt, refrigerant, and water. For heat transfer oils, which are light brown in color as shown in Fig. 1, the scale should be less than 1/50 to match Bo'. Moreover, the ratio of the *Gr*' number is much lower than that of other liquids so that the flow regime is significantly changed. Because it has the highest viscosity and lowest thermal conductivity among the candidate fluids, heat transfer oil is not suitable as a working fluid. Moreover, in terms of visualization, liquid metal is worse than other candidates because of its opacity. Heat transfer salts, which are green in Fig. 1, require a smaller length scale than water and are also opaque. Refrigerants, written in blue, are transparent but require a smaller length scale for identical Bo'. Ethanol has similar characteristics with refrigerants. Thus, refrigerant and ethanol have no advantage over water. Therefore, water is the best working fluid for simulating fluid in the aspect of visualization and length scale. Finally, the length scale difference between Wood's metal and water is decided to 14.1 : 1. Thermal properties of water and Wood's metal used in the present study were summarized in Table 1.

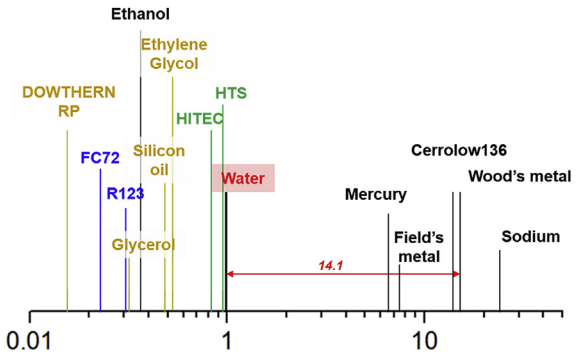

Fig. 1. Relative length scale for identical Bo'.

2.3. Experimental facility

The experimental facilities were designed as a 2-D slab model based on the RVACS operation conditions. The pair of facilities is called SINCRO-V, which stands for simulating natural circulation under RVACS operation-validation of the similarity law. As illustrated in Fig. 2, SINCRO-V simulates the characteristics of the RVACS. The overall reactor pool and flow path were simplified as a quarter circle pool and separator. Decay heat from the reactor core was simulated by a group of cartridge heaters in terms of volumetric heat generation. Cooling at the reactor vessel wall was simulated by the cooling wall in terms of temperature. Although cooling was described as heat flux in equation (3), it is better to represented as temperature in the aspect of its distribution and practicality. Under steady state, without significant of heat loss, the amount of cooling should be equal to heating amount so that similarity about average non-dimensional cooling heat flux is automatically achieved. Regard to heat flux distribution, temperature difference between the cooling wall and heat transfer coefficient are important. Temperature of the fluid is determined as multiplication of the reference temperature difference and non-dimensional temperature difference, as described in equation (12). So that distribution of the temperature difference along the cooling wall is automatically matched by the Bo' based similarity law itself. The local heat transfer coefficient is the function of the position, the temperature difference, and material properties. For its distribution, only temperature difference is matter because its relative position is maintained under isotropic scaling. Relative magnitude of the temperature difference could be maintained by controlling temperature. Additionally, temperature boundary condition has significant advantages in monitoring and controlling than heat flux boundary condition. Therefore, temperature boundary condition was used in the SINCRO-V experiment.

As illustrated in Fig. 2, the SINCRO-V facilities were designed in two-dimensional, slab model. Both Wood's metal and water facility had the geometrically scaled cross section with 14.1 : 1 of the length ratio, while the distance between slabs are kept identical. In the derivation of the similarity law, isotropic reduction of the scale reduction was assumed. Because it is two-dimensional facility, change of the phenomena could be neglected along thickness direction. Phenomena at the cross section of the 2-D slab are conserved while thickness of the slab changes. Therefore, the scale reduction in the SINCRO-V facility could be treated as isotropic scale reduction because change of the thickness and corresponding parameters did not affect two-dimensional phenomena. The specifications of each facility are summarized in Table 2. The radius of the pool, the main design parameter in SINCRO-V, was 1128 mm and 80 mm, each with 14.1:1 of length ratio. The width was fixed at 100 mm. Richardson number was maintained as unity for both facility by employing (4) and (6) under natural circulation. Pressure drop coefficient was assumed identical for both facility because cross sectional shape of the facilities was very similar, and their design was quite simple. Because volumetric heat generation rate was maintained for the convenience of the experiment, actual

Table 1
Summary of thermal properties of the water and Wood's metal.

	Water	Wood's metal
Melting point [°C]	0	80
Density [kg/m^3]	998	9500
Volumetric thermal expansion coefficient [1/K]	0.000207	0.000025
Thermal conductivity [W/m.K]	0.5985	13.5
Specific heat [J/kg.K]	4184.8	190
Dynamic viscosity [mPa.s]	1.002	4.0

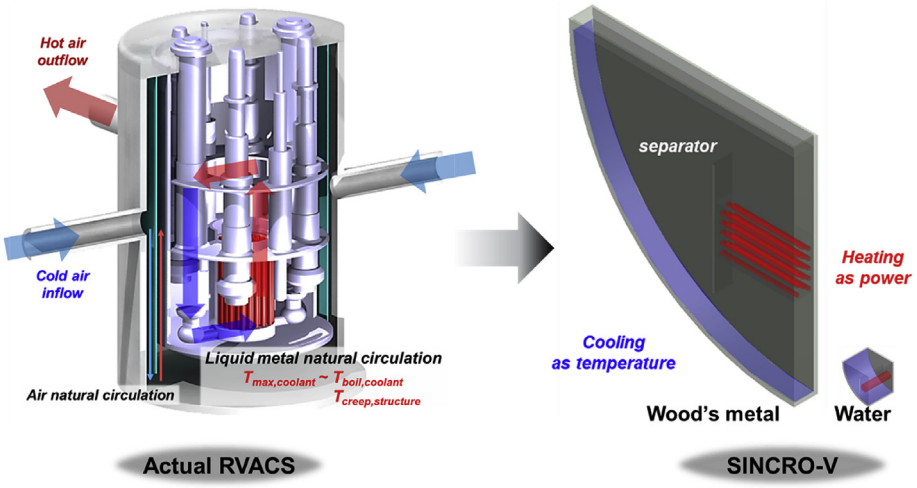

Fig. 2. Schematic of the SINCRO-V.

Table 2
Specifications of a pair of SINCRO-V.

Parameter	Wood's metal	Water
Radius	1128 mm 14.1 : 1	80 mm
Width	100 mm 1 : 1	100 mm
Power	20 kW 14.1^2 : 1	100 W
Bo'	1.394×10^8 1.06 : 1	1.398×10^8
ΔT_{ref}	3.776 °C 8.55 : 1	0.442 °C
q"$_{average}$ at cooling wall	112.9 kW/m^2 14.1 : 1	7.96 kW/m^2

power of each pair was proportional to their volume so that their ratio is the squared length ratio. However, for the calculation of the parameters, power of the Wood's metal facility was determined as 280 kW(~100 W x 14.1^3) according to the isotropic scaling assumption. In this scale difference, two Bo' were almost identical at a ratio of 1.06:1. In this scale difference, two Bo' were almost identical, as a ratio of 1.06 : 1. The corresponding reference temperature differences were 3.776 °C and 0.442 °C in the Wood's metal and water facility, respectively, with ratio of 8.55:1. The power and average cooling heat flux showed good accordance in both facility in the aspect of the non-dimensional heat source and sink, which were described in equation (9). To fill the natural circulation pool of the SINCRO-V Wood's metal facility, 970 kg of the Wood's metal was required, while the water facility required only 0.5 kg.

2.4. Experimental condition

The RVACS is designed to cool decay heat, which is a function of time after shutdown. From a long-term cooling perspective, a maximum of 1% of the total power is assumed as decay heat. The decay heat condition and corresponding power in the SINCRO-V Wood's metal and water facilities are summarized in Table 3. The time after shutdown and corresponding decay heat were obtained from the decay heat under the loss of flow accident condition of PGSFR [8].

Considering characteristics of the RVACS, cooling was performed at the cooling boundary at almost constant temperature. In both facilities, the authors focused on providing almost constant

Table 3
Summary of the test conditions.

Decay heat (time after shutdown)	Power in SINCRO-V	
	Wood's metal	Water
0.2% (90 days)	4 kW	20 W
0.4% (6.8 days)	8 kW	40 W
0.6% (1.5 days)	12 kW	60 W
0.8% (12.6 h)	16 kW	80 W
1.0% (5.5 h)	20 kW	100 W

temperature cooling. Especially in the Wood's metal facility, to cover the large heat flux variations along the cooling wall, boiling was selected as a cooling method. Boiling has the highest heat transfer coefficient, which increases as heat flux increases. Owing to the characteristics of boiling heat transfer, temperature variations along the cooling boundary were less than 5 °C in the experiment. Temperature at the inner side of the cooling wall was estimated approximately 16.7 °C higher than the outer temperature. However, only 110.59 °C was the maximum temperature among 16 thermocouples (every 6°) sheathed near the pool-side surface of the cooling wall, so that author used this value for the boundary temperature calculation. Temperature variation with the change of the angular position could be negligible due to characteristics of the boiling. In the water facility, a high flow-rate water jacket covered the cooling wall so that there was less than 5 °C of temperature variations along the boundary, which was observed at the three point at mid-plane of the cooling wall (10, 45, 80°). Considering the magnitude of the heat flux and observing point, temperature inside of the cooling wall could be treated as identical so that the maximum temperature (24.6 °C) was used as boundary temperature.

2.5. Uncertainty analysis

In this analysis, three parameters were used to analyze natural circulation: power, flow rate, and temperature. Power was controlled by the voltage, and the voltage uncertainty was 3.00%. The uncertainty of heater resistance was 0.14%; thus, total uncertainty in the power was 6.00%. Uncertainty of the heater resistance was 0.14%, thus, total uncertainty in the power. The flow rate is the flow rate of the coolant, which was used in the heat balance calculation. Uncertainties of the flowmeter, interface, and (analog

to digital) AD conversion were 0.30 L/min, 0.04%, and 0.02%, respectively. The total uncertainty of the flow rate was 0.30 L/min. For the temperature, the uncertainty factors were the thermocouple, compensation wire, room temperature, interface, and AD conversion with values 0.40%, 1.50 K, 0.50 K, 0.04%, and 0.02%, respectively. The total uncertainty of the temperature was 1.88–2.63 K.

Obviously, uncertainty range could be negligible for the high temperature. Regard to low temperature case, approximately 1.9 °C of the uncertainty range could be applied. Water temperature was translated to the Wood's metal temperature by equation (15), thus, temperature difference is important, not the temperature itself. Small temperature differences could be observed in the water case. For the 1.0% of the decay heat case, approximately 18 °C of the temperature difference was observed so that 1.9 °C of the uncertainty could be treated negligible. However, in case of the 0.2% case, approximately 5.7 °C of the temperature was observed. Here, uncertainty range was about 30% of the reading value. Although fraction of uncertainty was large, characteristics of both temperature and θ showed similar tendency to the other cases. Therefore, it was assumed that all the measured value was independent from the measurement uncertainty.

3. Results and discussion

3.1. Heat balance test

In the Wood's metal facility, the heat was intended to be removed only from the cooling surface, which was cooled by boiling heat transfer. It is well known that heat transfer performance under boiling is proportional to the cube of the superheat. In other words, the thermal resistance of the cooling wall significantly decreased as the system temperature increased. The thermal resistance of natural circulation decreased as the temperature difference increased, although the magnitude of decrease is much smaller than that of boiling. Considering the heat transfer characteristics of each surface, the amount of heat loss in the Wood's metal facility was smaller than in the high-power operation; however, the heat loss fraction was smaller during high-power operation. Heat loss was calculated by measuring the time it takes to consume 1 L of water for cooling. Originally, the facility had insulators with uniform thickness on all surfaces. However, insulation performance was poor; hence, insulators were added to the upper part of the facility. After the insulation was increased by more than 90%, as shown in Fig. 3, the following experiments were conducted under this condition.

Unlike the Wood's metal facility, the water facility was cooled by water cooling jacket and forced convection. Thus, the thermal resistance of the cooling side was almost constant, while the heat loss fraction was the largest in the highest-power case. Heat loss in the water facility was calculated by flow rate and temperature increase through the coolant at the water jacket. Considering the uncertainty range in Table 4, the uncertainty of heat loss calculation increased as the power level decreased. For these reasons, heat loss was evaluated only in the 100 W case, which was expected to have the highest heat loss. The observed heat loss rate was approximately 90.3%.

3.2. Temperature distribution characteristics in the pool

Fig. 4 shows the representative temperature distributions under 1% of decay heat condition, 20 kW, and 100 W in the Wood's metal and water facilities, respectively. Overall, both facilities showed similar temperature distribution characteristics. The temperature was stratified in the whole pool and was clearly observed in the

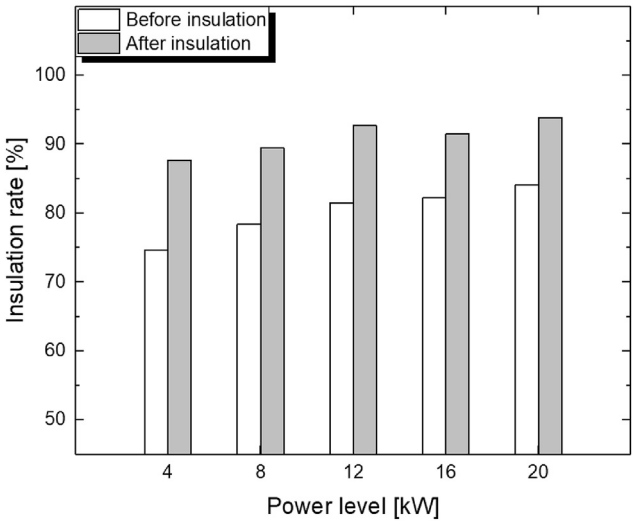

Fig. 3. Insulation rate in the Wood's metal facility at various power levels.

Table 4
Summary of uncertainty analysis.

Category	Contributor	Magnitude
Power	Voltage	3.00%
	Resistance	0.14%
	Total	6.00%
Flowrate	Flowmeter	0.30 L/min
	I/O interface	0.04%
	AD conversion	0.02%
	Total	0.30 L/min
Temperature	Thermocouple	0.40%
	Compensation wire	1.50 K
	Room temperature	0.50 K
	I/O interface	0.04%
	AD conversion	0.02%
	Total	1.88–2.63 K

temperature of a group of vertically-arranged thermocouples. In terms of natural circulation flow, the hot region was generated after the heating zone and expanded into the upper plenum. The hot fluid in the upper plenum flowed downward near the cooling wall while cooling down. This downward flow entrained the stratified temperature profile; therefore, all the temperature points near the cooling wall showed slightly higher values than those at the vertically-arranged observation points with the same height. The downward flow continued along the cooling wall, and then separated from the wall at the same height as the bottom of the separator. Separation of the downward flow was indicated by the drastic change in temperature distribution at the bottom of the pool. At the end of the vertically-arranged temperature points, in the case of the Wood's metal, the temperature was 141.9 °C. This is a decrease of over 45 °C from the temperature point above of 187.9 °C, while other temperature differences between next above points were approximately 20 °C. These vertically-arranged temperature points were installed at the same pitch; thus, the temperature gradient drastically changed in this region. Temperature change history along the cooling wall showed a similar tendency as the vertically-arranged points: significantly larger temperature decrease was observed between two points at the bottom. Finally, at approximately 185 °C of inlet temperature, it was reasonable to exclude the lowest temperature point from the natural circulation flow path. The estimated flow including separation of the downward flow from the wall is illustrated in Fig. 4 with gray arrows. The water

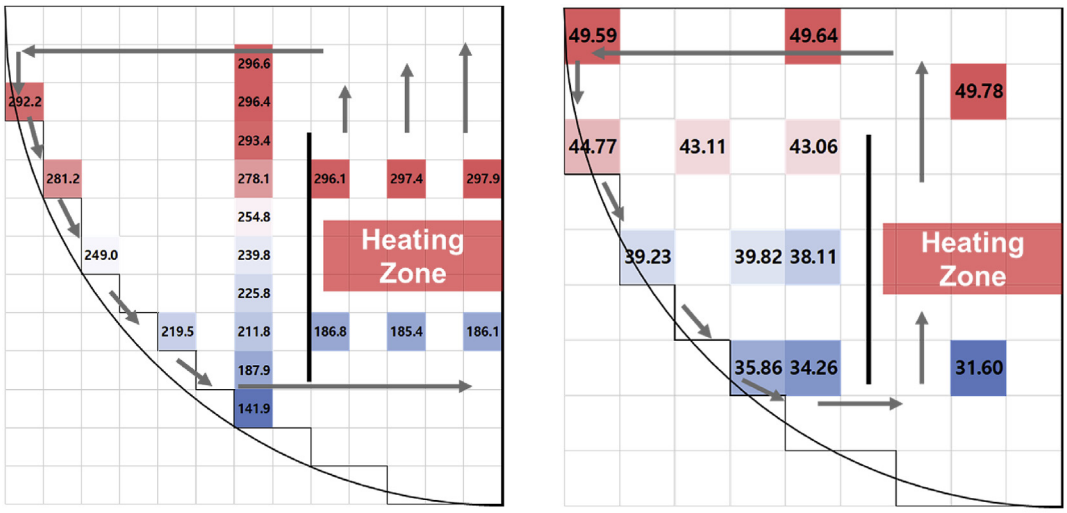

Fig. 4. Temperature distribution in the pool under 1% of decay heat condition.

facility had some limitations with regard to the installation of thermocouples because of its small size, resulting in the small number of observation points. Nonetheless, the following temperature distribution characteristics of the Wood's metal facility were also observed in the water facility: hot region in the upper plenum, temperature stratification, and entrainment of stratified temperature field by natural circulation flow near the cooling wall. However, separation of the downward flow from the wall was not clearly observed in the water facility. The sudden decrease in temperature was not observed, and the temperature at the inlet of the heating zone was lower than that at the lowest and vertically-arranged observation point of the wall. This could be attributed to the effect of non-identical *Gr*'. As illustrated in Fig. 5, at the length scale of 14.1, the Bo' in the Wood's metal facility and water facility are identical, as intended. However, *Gr*' in the Wood's metal facility was approximately 16,000 times larger than that in the water facility. This means that the effects of buoyancy force and corresponding inertia of natural circulation were stronger in the Wood's metal facility. In other words, the intensity of natural circulation flow was lower in the water facility. Therefore, flow separation was delayed by the weak deriving force of natural circulation, and reduced thermal mixing was achieved in the lower plenum of the water facility. With regard to the natural circulation of liquid metal, the water showed good agreement with liquid metal qualitatively, except for phenomena related to flow inertia.

3.3. Effect of decay heat

To compare temperature more quantitatively, some representative points were selected, and the temperatures were compared at these points. The locations of the points are illustrated in Fig. 6. The core inlet and outlet were selected for observation of the minimum and maximum temperatures. Four points in the middle of the pool and four points in the cooling wall region were selected to observe the stratification and change history of temperature during the cooling process, respectively.

Fig. 7 shows the temperature distribution in the pool with different decay heat levels. In both the Wood's metal and water, the temperature distribution characteristics did not change even with changes in decay heat level. When the decay heat changed, the

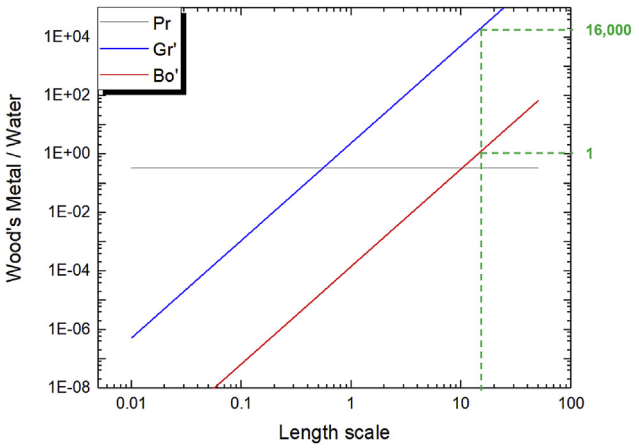

Fig. 5. The behavior of important nondimensional numbers along the length scale.

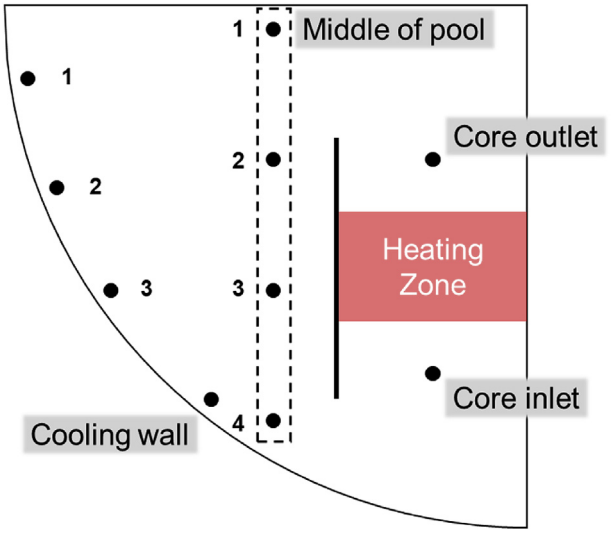

Fig. 6. Location of selected temperature point for the graph.

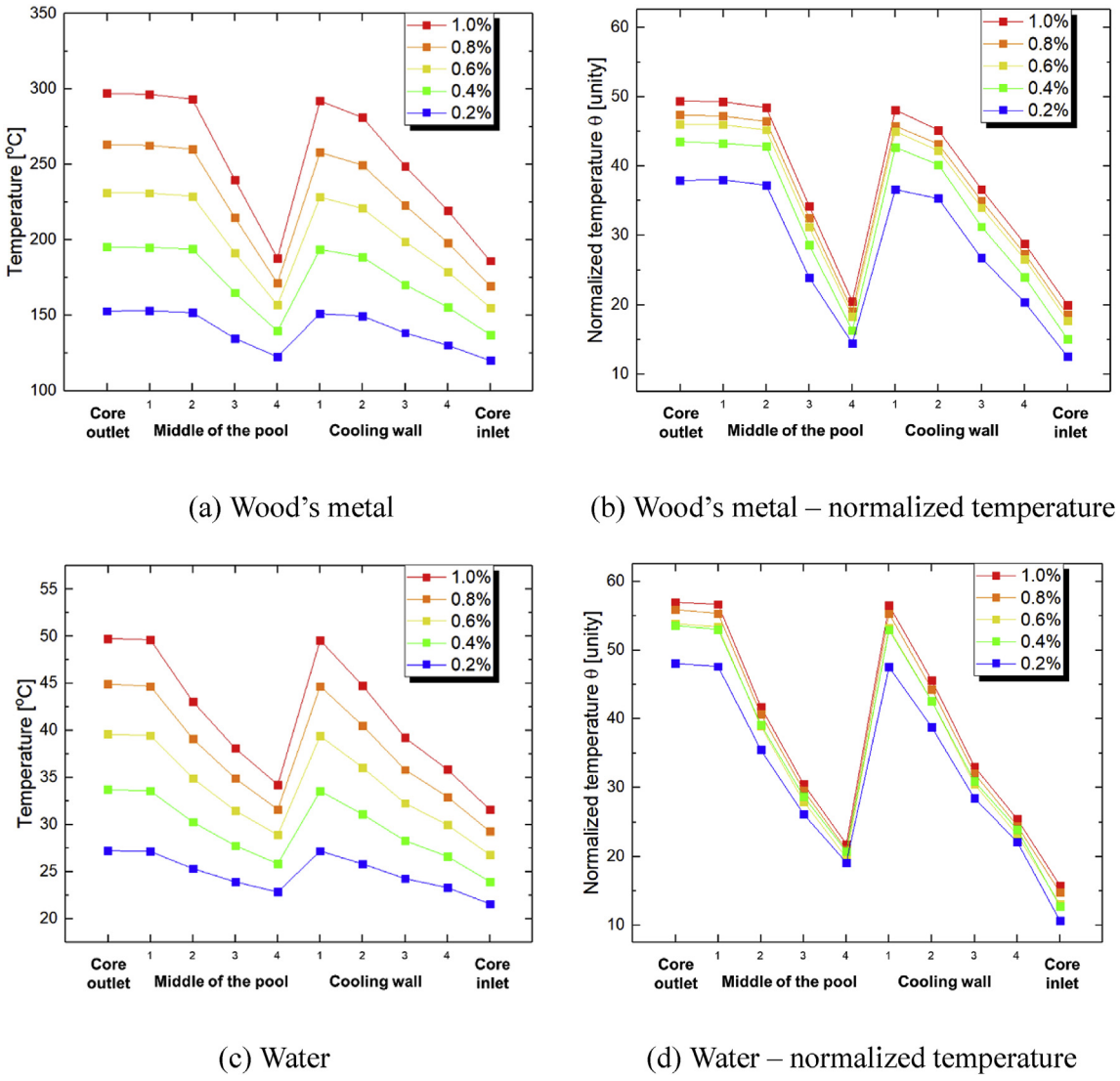

Fig. 7. The temperature and normalized temperature at the selected points with various decay heat levels.

magnitude of the temperature also changed while its tendency was maintained. Therefore, the decay heat only influenced the magnitude of the temperature; it did not affect the temperature distribution characteristics under the given decay heat level conditions.

Overall trend was the same to its temperature graph, however, some additional points could be observed by the normalized graph, effect of the boundary condition and the property change. The SINCRO-V experiment intended to have constant temperature boundary condition, however, it was not fully achieved due to practical limitation. Boundary temperature was determined as the maximum temperature observed in the experiment in all cases. If boundary temperature was overestimated than actual, according to equation (12), normalized temperature (θ) would be underestimated and vice versa. In (b) of Fig. 7, there was significant decrease of the normalized temperature. The maximum θ was 49.4 and it decreased to 19.9 at the core inlet in the 1.0% power case, while maximum θ was 38.0 and minimum θ was 12.5 in the 0.2% case. The θ difference between the maximum and the minimum was decreased, and overall magnitude of the θ was decreased more in 0.2% power case.

Change of the overall magnitude was the global phenomena. As described in the above, underestimation of the boundary temperature made θ increase. Informed in section 2.4, boundary temperature was determined as the maximum cooling wall temperature observed in the experiment, which was lower than calculated value. Order of the error was approximately 20 °C in the 1.0% case and it corresponds to 5.5 of θ, which was still not enough value to explain such a large θ difference. It suggested that there was still disagreement of θ, although boundary temperature was perfectly given. Exclusion of the near wall heat transfer could be suggested as another reason for the overall magnitude change. Temperature increase at the near wall region, especially cooling wall, became more considerable in the higher power case. It could be negligible in the lower power case, which had small heat flux at the cooling boundary. However, it was neglected for the all case, therefore, it made significant error in the higher power case. Change of the thermal properties of the working fluid also caused increase of the overall temperature. Generally, thermal conductivity of the metal decreases as temperature increases. This also caused more temperature increase in the high-power case.

Change of the θ difference between the maximum and the minimum means less thermal mixing by the natural circulation. As temperature increase, viscosity of the Wood's metal decrease, which made more intense natural circulation and thermal mixing. Current similarity law focused on the temperature, and flow related parameters were not considered. Therefore, increase of the thermal

mixing and intensity of the natural circulation was neglected. In addition, properties change along the temperature also made θ difference larger. As discussed in the previous paragraph, decreased thermal conductivity at the higher temperature cause additional temperature increase.

Different to Wood's metal, (b) in the water facility (d), discordance among the different power case was not significant. For the change of the overall magnitude of the θ, several effects discussed in the Wood's metal case, could be negligible. In water case, boundary temperature was determined as almost same with actual boundary temperature so that the error from the determination of the boundary temperature could be removed. For the near wall heat transfer, although magnitude of the heat flux was much lower than that of the Wood's metal, thermal conductivity of the water was also much lower. Different to Wood's metal, thermal conductivity of the water slightly increases about 7% as temperature increases, in the current experimental range. It provided adverse effect to θ increase at the high power. Therefore, overall θ increase in the high power was much less significant compared to Wood's metal.

Regard to change of the θ difference between the maximum and the minimum, its magnitude was smaller than that of the Wood's metal. As temperature increases, decreased viscosity made more intense natural circulation and thermal mixing. However, thermal conductivity of the water slightly increases as temperature increases. Therefore, two factors acted in the opposite direction, magnitude of the θ difference increase along the power was less significant than that of the Wood's metal. However, magnitude of the change of the viscosity was much significant compared to the change of the thermal conductivity, θ difference was still increased as temperature increases.

3.4. Prediction of the Wood's metal temperature and validation

As described in Section 2.1, the Wood's metal temperature could be predicted by the water experiment and the reference temperature in each system using equation (15). Specifically, the temperature difference between a certain point in the Wood's metal and its boundary could be predicted by the temperature difference between the corresponding point in the water and the boundary of the water pool, as expressed by equation (16).

$$\left(T_{Wood's\ metal} - T_{boundary,\ Wood's\ metal}\right) = \frac{\Delta T_{reference,\ Wood's\ metal}}{\Delta T_{reference,\ water}} \times \left(T_{water} - T_{boundary,\ water}\right) \tag{16}$$

Both the Wood's metal and water facility were designed to have constant boundary temperature on the cooling surface. However, heat flux variations along the angular direction caused fluctuations of the boundary temperature. In case of 1.0% of decay heat condition, temperatures from 101.6 °C to 110.6 °C were observed along the angular position in the Wood's metal facility, while 19.1 °C–24.6 °C were observed in the water facility. The boundary temperature was lower at the lower part of the cooling boundary. Here, the boundary temperature was assumed to be the maximum temperature along the angular position. This is because the maximum temperature point is the temperature at the main cooling point and could reflect the change in boundary temperature along the decay heat level. As discussed in the previous section, the effect of decay heat on temperature distribution tendency could be negligible; hence, the 1.0% of decay heat condition was analyzed as a representative.

The actual temperature of the Wood's metal in the experiment and predicted temperature by the water were compared at selected points. As shown in Fig. 8, the water experiment predicted the Wood's metal temperature accurately. The maximum temperature, which was observed at the core outlet, was 297.1 °C in the Wood's metal experiment, while the water experiment predicted 325.6 °C, an overestimation of 14.4%. The minimum temperatures observed at the core inlet were 186.1 °C and 170.2 °C in the Wood's metal experiment and water simulating experiment, respectively. This is an underestimation of 18.5%, and this point had the largest error. The stratified temperature field could be observed by the points in the middle of the pool. Point 1 in the middle of the pool showed similar temperature with the core outlet. In this region, the temperature decreased as the point went down. The thickness of the hot region in the upper plenum was underestimated in the water experiment. In the Wood's metal experiment, the temperature at points 1 and 2 in the middle of the pool was similar. However, in the water facility, temperature greatly decreased at the point 2 compared with point 1. This means that hot flow from above the core to the cooling wall was shallower in the water experiment. At points 3 and 4, the predicted temperature showed good agreement with the Wood's metal data. The temperature gradient was smaller in the water experiment; however, considering the overestimated upper plenum temperature and underestimated thickness of the hot region, the temperature in the middle of the pool at point 4 showed good agreement with the actual Wood's metal temperature. Point 1 in the cooling wall was in the hot region in the upper plenum; hence, it showed overestimated temperature like the core outlet and point 1 in the middle of the pool. The temperature change at the points along the cooling wall indicates the cooling rate along the cooling wall. The rate of temperature decrease along the wall was overestimated in the water experiment such that the temperature at point 4 was underestimated, while point 1 was overestimated. There were few local errors in prediction: overestimation of the maximum temperature by 14.4% and underestimation of the minimum temperature by 18.5%. Despite these local errors, it can be concluded that the overall temperature was accurately predicted, and the tendency of temperature distribution was accurately reproduced. Local errors were further discussed in the following section.

Errors at each point and various decay heat levels are shown in Fig. 9. As discussed in the previous figures, the decay heat did not affect the characteristics of natural circulation, which was confirmed by the error graph. In all power ranges and hot regions such as the core outlet and upper plenum, point number 1 in the middle of the pool and cooling wall was overestimated. The core

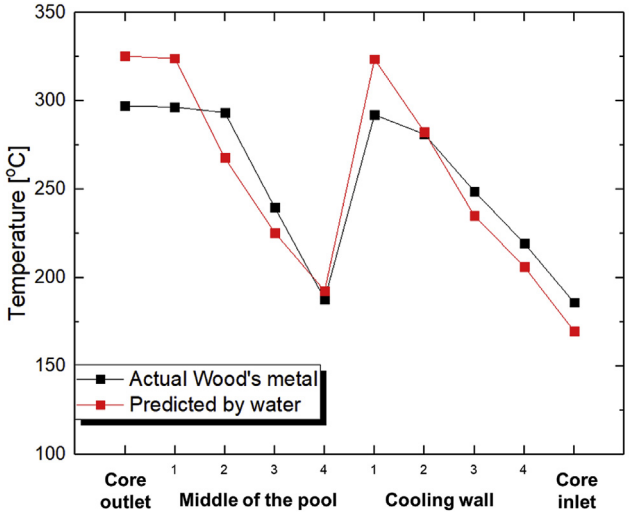

Fig. 8. Actual and predicted Wood's metal temperature in 1.0% of decay heat.

inlet was always underestimated, which means that the temperature distribution was more polarized. The hot points were overestimated, and cold points were underestimated, which can be attributed to the difference in the *Gr*'. As shown in Fig. 5, *Gr*' in the Wood's metal facility was larger than in the water facility. Smaller *Gr*' caused an increase in the pressure drop coefficient (Ri) as well as reduced thermal mixing due to the less intense natural circulation flow. Theoretically, the pressure drop coefficient is inversely proportional to the Reynolds number, which can be translated as the *Gr*' in natural circulation in terms of flow inertia. The water facility had smaller *Gr*' than in the Wood's metal facility; thus, it can be said that the water facility had a larger pressure drop than the Wood's metal facility. Therefore, the temperature difference at the inlet and outlet was slightly exaggerated.

Overall, the temperature was overestimated as decay heat level decreased. As discussed in the normalized temperature section, there were a greater number of temperature increasing factors in the Wood's metal case: boundary temperature determination, ignorance of the near wall heat transfer, property change especially thermal conductivity, thermal mixing intensity change by decrease of viscosity. However, in case of the water, boundary temperature determination factor became less significant and increase of the thermal conductivity acted in the opposite direction. Therefore, water experiment tended to relatively underestimate Wood's metal temperature in the higher power condition. This caused an upward shift of graph as the power level decreased in Fig. 9. The constant boundary assumption and the representative value for boundary temperature is the main reason for this kind of error.

The effect of the error in the boundary condition also changed with decay heat level. With regard to decay heat, 1.0%, 0.8%, and 0.6% of decay heat levels showed similar error distribution tendency. However, 0.4% and 0.2% exhibited slightly different error behavior, which is related to the temperature distribution along the cooling boundary. For the Wood's metal facility, the maximum temperature difference along the wall was in the order of a few degrees, from 2.3 °C to 9.0 °C along the power level. It could be negligible compared with the temperature difference between the boundary and the pool, which was approximately 50 °C and 200 °C in maximum in 0.2% and 1.0% of the decay heat, respectively. However, in the water facility, the wall temperature variations ranged from 1.1 °C to 4.6 °C. The maximum temperature difference between the boundary and the pool was approximately 10 °C and 25 °C in 0.2% and 1.0%, respectively. Comparing the order

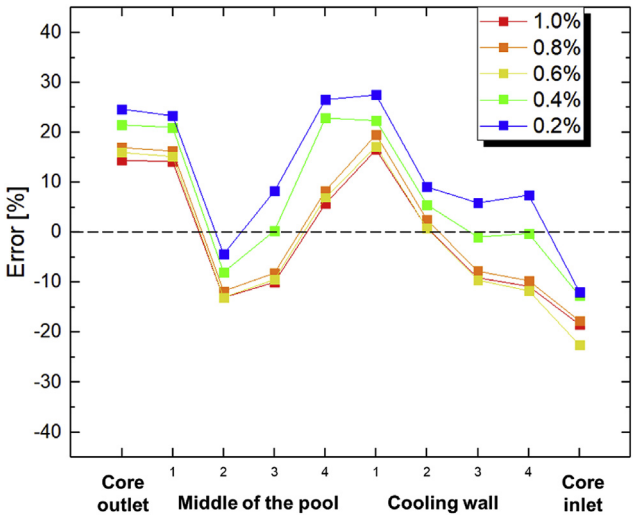

Fig. 9. Local prediction error with the various decay heat level.

of the pool temperature distribution and temperature variations along the cooling wall, temperature variations along the cooling wall became more significant as the power level increased. Therefore, high-power conditions like 0.6%, 0.8%, and 1.0% led to the underestimation of pool temperature in the lower plenum because of temperature variations along the cooling wall. In low-power cases, 0.4% and 0.2%, the magnitude of boundary temperature variations was less significant than that in high-power cases; hence, underestimation of temperature in the lower plenum was not observed. In conclusion, the overall temperature gradient at the top and bottom of the pool was influenced by uneven boundary temperature, which caused overprediction of the temperature difference between the top and bottom of the pool in high-power cases.

4. Conclusion

To validate the similarity law of natural circulation with two fluids having extremely different Pr, a pair of SINCRO-V facilities were designed as the two-dimensional slab model. Wood's metal was selected as the representative fluid for liquid metal while water was selected for the simulation of liquid metal. The Bo' was the main similarity parameter. The length scale difference between the Wood's metal facility and water facility was 14.1:1.

In the SINCRO-V, the following temperature distribution characteristics in the pool under natural circulation were observed: hot region in the upper plenum, entrainment of temperature field by downward flow, and overall temperature stratification. Changes in the decay heat caused changes in the temperature distribution and it could be more clearly recognized from the normalized temperature (θ). The temperature distribution characteristics did not change significantly at decay power levels from 0.2% to 1.0%, however, overall magnitude of the θ and the maximum θ difference in the pool was changed significantly in the Wood's metal case. Underestimated boundary temperature, ignorance of the near wall heat transfer, and ignorance of the property change of the material with temperature caused increase of the θ in the high Wood's metal case. The maximum θ difference decreased at the high power due to increase of the thermal conductivity and due to more intense natural circulation and thermal mixing. In contrast, for the water case, boundary temperature effect could be negligible. Near wall heat transfer was still significant, however, change of thermal conductivity with temperature acted oppositely, so that overall magnitude of the θ increase along the power was much smaller. For change of the maximum θ difference, property change and increase of thermal mixing acted in the opposite direction, thus, magnitude of the θ difference increase along the power was smaller than that of the Wood's metal.

Quantitatively, the water experiment predicted the Wood's metal temperature with acceptable errors. The smaller *Gr*' in the water facility increased the relative pressure drop, and led to the overestimation of the temperature difference between the core inlet and outlet. There were a greater number of temperature increasing factors in the Wood's metal case: boundary temperature determination, ignorance of the near wall heat transfer, property change, thermal mixing intensity change. However, in case of the water, boundary temperature determination factor became less significant and property change acted in the opposite direction. Therefore, water experiment tended to relatively underestimate Wood's metal temperature in the higher power condition. Despite these errors, the water experiment predicted the Wood's metal temperature with an error of less than 27%. Therefore, the natural circulation of liquid metal can be simulated by water despite extreme difference of Pr.

Declaration of competing interest

We certify that there is no conflict of interest including any financial, personal or other relationships with other people or organizations within three years of beginning the submitted work that could inappropriately influence, or be perceived to influence, our work.

Acknowledgment

.This work was supported by the Nuclear Energy Research Program and Basic Science Research Program through the National Research Foundation of Korea (NRF) funded by the Ministry of Science, ICT, and Future Planning (No. 2018M2A8A4031186, 2017R1A2B2008031, 2017M2A8A2018595).

Nomenclature

Bo'	modified Boussinesq number [1] $Bo' = \left(\frac{\beta g}{\rho c_p}\right)^{2/3} \frac{L^{4/3} Q^{2/3}}{\alpha^2}$
Gr'	modified Grashof number [1] $Gr' = \left(\frac{\beta g}{\rho c_p}\right)^{2/3} \frac{L^{4/3} Q^{2/3}}{\nu^2}$
L	characteristic length [m]
P	pressure [Pa]
Q	heat generation rate [W]
Q″	heat flux [W/m^2]
Q_0	volumetric heat generation rate [W/m^3]
T	temperature [K]
T_0	temperature at the arbitrary reference point [K]
T*	non-dimensionalized temperature [1] $T^* = (T - T_0)/\Delta T_{ref}$
c_p	specific heat [J/kg.K]
g	gravitational acceleration [m/s^2]
t	time [s]
t*	non-dimensionalized time [1] $t^* = t/t_{ref}$
u_i	velocity [m/s]
u_i*	non-dimensionalized velocity [1] $u_i^* = u_i/u_{ref}$
x_i	Cartesian co-ordinates [m]
x_i*	non-dimensionalized Cartesian co-ordinates [m] $x_i^* = x_i/L$
α	thermal diffusivity [m^2/s]
β	volumetric thermal expansion coefficient [1/K]
δ_{ij}	Kronecker's delta [1].
θ	Non-dimensionalized temperature [1].
ν	kinematic viscosity [m^2/s]
ρ	density [kg/m^3]

Appendix A. Supplementary data

Supplementary data to this article can be found online at https://doi.org/10.1016/j.net.2020.03.005.

References

[1] E.E. Feldman, D. Mohr, L.K. Chang, H.P. Planchon, E.M. Dean, P.R. Betten, EBR-II unprotected loss-of-heat-sink predictions and preliminary test results, Nucl. Eng. Des. 101 (1987) 57–66.
[2] H.P. Planchon, J.I. Sackett, G.H. Golden, R.H. Sevy, Implications of EBR-II inherent safety demonstration test, Nucl. Eng. Des. 101 (1987) 75–90.
[3] W.K. Lehto, R.M. Fryer, E.M. Dean, J.F. Koenig, L.K. Chang, D. Mohr, E.E. Feldman, Safety analysis for the loss-of-flow and loss-of-heat sink without scram tests in EBR-II, Nucl. Eng. Des. 101 (1987) 35–44.
[4] F. Yamada, Y. Fukano, H. Nishi, M. Konomura, Development of natural circulation analytical model in super-COPD code and evaluation of core cooling capability in monju during a station blackout, Nucl. Technol. 188 (2014) 292–321.
[5] T. Ishizu, H. Endo, Y. Shindo, K. Haga, An evaluation of passive safety features of the Japanese prototype LMFBR monju, in: Proceedings of the 11th International Topical Meeting on Nuclear Reactor Thermal Hydraulics (NURETH-11), Avignon, France, 2005.
[6] M. Sadawa, H. Arikawa, N. Mizoo, Experiment and analysis on natural convection characteristics in the experimental fast reactor joyo, Nucl. Eng. Des. 120 (1990) 341–347.
[7] J. Yoo, J. Chang, J.Y. Lim, J.S. Cheon, T.H. Lee, S.K. Kim, K.L. Lee, H.K. Joo, Overall system description and safety characteristics of prototype gen IV sodium cooled fast reactor in Korea, Nucl. Eng. Technol. 48 (2016), 10595-11070.
[8] K.L. Lee, K.S. Ha, J.H. Jeong, C.W. Choi, T.K. Jeong, S.J. Ahn, S.W. Lee, W.P. Chang, S.H. Kang, J.Y. Yoo, A preliminary safety analysis for the prototype gen-IV sodium-cooled fast reactor, Nucl. Eng. Technol. 48 (2016) 1071–1082.
[9] E. Hourcade, F. Curnier, T. Mihara, B. Farges, J.F. Dirat, A. Ide, ASTRID Nuclear Island Design: advances in French-Japanese joint team development of decay heat removal systems, in: Proceedings of the 2016 International Congress on Advances in Nuclear Power Plants (ICAPP 2016), San Francisco, CA, 2016.
[10] C.F. Smith, W.G. Halsey, N.W. Brown, J.J. Sienicki, A. Moisseytsev, D.C. Wade, SSTAR: the US lead-cooled fast reactor (LFR), J. Nucl. Mater. 376 (2008) 255–259.
[11] J. Wallenius, E. Suvdantsetseg, A. Fokau, ELECTRA: European lead-cooled training reactor, Nucl. Technol. 117 (2012) 303–313.
[12] H.A. Abderrahim, P. D'hondt, MYRRHA: a European experimental ads for R&D Applications status at mid-2005 and prospective towards implementation, J. Nucl. Sci. Technol. 44 (2007) 491–498.
[13] N. Tanaka, S. Moriya, S. Ushijima, T. Koga, Y. Eguchi, Prediction method for thermal stratification in a reactor vessel, Nucl. Eng. Des. 120 (1990) 395–402.
[14] Y. Ieda, H. Kamide, H. Ohshima, S. Sugawara, H. Ninokata, Strategy of experimental studies in PNC on natural convection decay heat removal, in: Proceedings of IAEA-IWGFR Specialists' Meeting on "Evaluation of Decay Heat Removal by Natural Convection", O-arai, Japan, 1993.
[15] A. Ono, H. Kamide, J. Kobayashi, N. Doda, Osamu Watanabe, An experimental study on natural circulation decay heat removal system for a loop type fast reactor, J. Nucl. Sci. Technol. 53 (2016) 1385–1396.
[16] G. Coccoluto, P. Gaggini, V. Labanti, M. Tarantino, W. Ambrosini, N. Forgione, A. Napoli, F. Oriolo, Heavy liquid metal natural circulation in a one-dimensional loop, Nucl. Eng. Des. 241 (2011) 1301–1309.
[17] C.C. Yue, L.L. Chen, K.F. Lyu, Y. Li, S. Gao, Y.J. Liu, Q.Y. Huang, Flow characteristics of natural circulation in a lead–bismuth eutectic loop, Nucl. Sci. Technol. 28 (2017) 28–39.
[18] K.H. Ryu, B.M. Ban, T.H. Lee, J.H. Lee, S.H. Lee, J.H. Cho, S.H. Ko, J.H. Kim, Natural circulation characteristics under various conditions on heavy liquid metal test loop, Int. J. Therm. Sci. 132 (2018) 316–321.
[19] S. Grewal, E. Gluekler, Water simulation of sodium reactors, Chem. Eng. Commun. 17 (1982), 3443-4360.
[20] Y. Eguchi, H. Takeda, T. Koga, N. Tanaka, K. Yamamoto, Quantitative prediction of natural circulation in an LMFR with a similarity law and a water test, Nucl. Eng. Des. 178 (1997) 295–307.
[21] H. Hoffman, D. Weinberg, Y. Ieda, K. Marten, H. Tschöke, H.H. Frey, Kurt Dres, Thermohydraulic investigations of decay heat removal systems by natural convection for liquid-metal fast breeder reactors, Nucl. Technol. 88 (1989) 75–88.
[22] H. Hoffman, D. Wienberg, R. Webstar, Investigation on natural convection decay heat removal for the EFR – status of the Program, in: Proceedings of IAEA-IWGFR Specialists' Meeting on "Passive and Active Safety Features of LMFRs", Oarai, Japan, 1991.
[23] D. Wienberg, H. Hoffman, H. Ohira, G. Schnetgöke, The status study using RAMONA and NEPTUN models on decay heat removal by natural convection for the European fast reactor, in: Proceedings of IAEA-IWGFR Specialists' Meeting on "Evaluation of Decay Heat Removal by Natural Convection in Fast Reactor", Mito, Japan, 1993.
[24] D. Wienberg, K. Rust, H. Hoffmann, Overview Report of RAMONA-NEPTUN Program on Passive Decay Heat Removal, Report FZKA 5667, Forschungszentrum Karlsruhe, 1996.
[25] M. Akutsu, Y. Okabe, K. Satoh, H. Kamide, K. Hayashi, N. Naohara, K. Iwashige, Y. Shibata, Study of thermal-hydraulic characteristics during decay heat removal in a pool-type fast breeder reactor, Nucl. Technol. 98 (1992) 14–26.
[26] H. Takeda, T. Koga, Study on similarity rule for natural circulation water test of LMFBR, in: Proceedings of IAEA-IWGFR Specialists' Meeting on "Evaluation of Decay Heat Removal by Natural Convection in Fast Reactor", Mito, Japan, 1993.
[27] H. Takeda, T. Koga, O. Watanabe, Experimental and computational simulation for natural circulation in an LMFBR, Nucl. Eng. Des. 140 (1993) 331–340.
[28] K. Rust, H. Tschöke, D. Weinberg, Influence of the position and number of decay heat exchangers on the thermal hydraulics of a slab test facility: a comparison of analytical and experimental data, Exp. Therm. Fluid Sci. 9 (1994) 413–425.
[29] V.M. Mente, G.K. Pandey, I. Banerjee, S. Ajesh Kumar, G. Padmakumar, K.K. Rajan, Experimental studies in water for safety grade decay heat removal of prototype fast breeder reactor, Ann. Nucl. Energy 65 (2014) 114–121.
[30] T. Murakami, Y. Eguchi, K. Oyama, O. Watanabe, Reduced-scale water test of natural circulation for decay heat removal in loop-type sodium-cooled fast reactor, Nucl. Eng. Des. 288 (2015) 220–231.
[31] A. Ono, A. Kurihara, M. Tanaka, H. Oshima, H. Kamide, Study on Reactor Vessel Coolability of Sodium-Cooled Fast Reactor under Severe Accident Condition – Water Experiments Using a Scale Model -, ICAPP 2017, Fukui and Kyoto, Japan, 2017.
[32] P. Planquarta, K. van Tichelen, Experimental investigation of accidental scenarios using a scale water model of a HLM reactor, Nucl. Eng. Des. 346 (2019) 10–16.